Rocky Worlds DDT: JWST/MIRI Checkpoint 2 Report for GJ 3929 b

Joshua Lothringer, Tyler Baines, Achrène Dyrek, Joseph Filippazzo, Douglas Long, Elena Manjavacas, Brett Morris, Ian Wong | *JWST Data Analysis Team*

Taylor James Bell | *JWST Data Analysis Team Lead*

Néstor Espinoza, Hannah Diamond-Lowe | *RWDDT CIT Leads*

June 23, 2026

The Rocky Worlds Director's Discretionary Time (RWDDT) program observed the exoplanet GJ 3929 b using MIRI Imaging photometry with the F1500W filter with the goal of measuring four secondary eclipses. We present here an analysis of the Checkpoint 2 dataset (all four eclipses) by the JWST Data Analysis Team. This work builds upon the Checkpoint 1 analysis that considered the first two eclipses of GJ 3929 b. We analyzed the data with different assumptions for the orbital solution (circular v.s. eccentric), different levels of time-series trimming, and different systematics models. Overall, we find that our joint-fit's precision is consistent with the precision we had aimed for with this 4-eclipse observation campaign.

1 Data Analysis

The JWST Data Analysis Team within the RWDDT's Core Implementation Team conducted a detailed analysis of the four Checkpoint 2 eclipses of GJ 3929 b individually as well as jointly. T. Baines and A. Dyrek independently analyzed Observation 1, and I. Wong and J. Filippazzo analyzed Observation 2, D. Long and I. Wong analyzed Observation 3, and J. Lothringer and E. Manjavacas analyzed Observations 4 & 5. The last eclipse consisted of two contiguous visits, split because the long baseline exceeded the maximum number of frames allowed in an individual exposure. As was noted in the report for Observations 4 & 5, this multi-visit strategy was found to be sub-optimal, and in the future we will instead employ a multi-exposure strategy (only falling back to using multiple visits if necessary due to extremely long observations).

For all four eclipses, the data analysts tested fits with different linear decorrelation methods (against PSF centroid positions and widths), with and without a Gaussian Process (GP) regression model as a function of time, and circular vs. eccentric solutions. All reductions and fitting were done with the Eureka! data analysis pipeline version 1.4.dev106+g3a6724481 (Bell et al., 2022).

1.1 Individual Visit Fits

We briefly summarize the results of the individual eclipse analyses here. For further details, see the Observation 1 Data Analysis, Observation 2 Data Analysis, Observation 3 Data Analysis, and Observation 4 Data Analysis report.

For all observations, we explored circular vs. eccentric orbits, as archival data was not able to tightly constrain the planet's orbital eccentricity. Unsurprisingly, we found

that we could not meaningfully constrain both the eclipse depth and the orbital eccentricity when analyzing only one eclipse at a time, so for each individual fit we chose to impose a mid-eclipse timing prior based on R. Cooper's circular-orbit global fitting results (performed prior to scheduling all GJ 3929 b eclipse observations).

The Observation 1 analyses recovered eclipse depths consistent with 0 ppm and with relatively large error bars that spanned both bare rock and atmospheric scenarios for the planet, although the eclipse depth and timing were found to be method and assumption dependent. Without a GP, the fitted eclipse depth was found to be 305 ± 35 ppm, which is considerably higher than the maximum expected eclipse depth for GJ 3929 b of ∼145 ppm, assuming zero albedo and zero recirculation (Espinoza et al., in prep.). Meanwhile, our fiducial fit that included a GP ended up with a suppressed eclipse depth and inflated eclipse depth uncertainties.

For Observation 2, our analyses also yielded eclipse depths consistent with 0 ppm with relatively large error bars, while also not being meaningfully inconsistent with the maximum-expected eclipse depth. The amplitude of the best-fit GP term ranged from 50 to 100 ppm — comparable to the expected eclipse depth for GJ 3929 b. These results suggest the presence of time-correlated noise hindering our ability to constrain both the mid-eclipse time and the eclipse depth from only a single visit.

For Observation 3, we found a much more statistically significant eclipse compared to the previous eclipses at about 180±35 ppm. Reductions from the two analysts resulted in consistent results despite removing different amounts of initial integrations (50 versus 800) and using different source aperture+background annulus pairs.

For Observations 4 & 5, the analysis was complicated by the mid-observation visit gap, which occurred just prior to the expected location of the eclipse in a circular orbit scenario, but during the eclipse in the moderately-eccentric scenario. Because of ramp-like behavior after the visit gap, data from Observation 4 were discarded and GPs were included in the fiducial fit, resulting in a large, but poorly constrained eclipse depth of about 200 ± 130 ppm.

For Observations 3–5, we also switched from using the newer CRDS context file `jwst_1464.pmap` compared to `jwst_1364.pmap`, which was used for Observations 1–2. The main impact of this newer pmap is that v1.0 of the Observation 1–2 HLSPs had absolutely-calibrated stellar fluxes that were low by ∼10% because of an overly aggressive bad-pixel mask used by `jwst_1364.pmap`. As a result, we also issued updated v1.0.1 HLSPs for Observations 1–2, where only the stellar flux measurements were updated, using the newer `jwst_1464.pmap`.

1.2 Checkpoint 2 Joint Fits

For all data in Checkpoint 2, we used the fiducial aperture photometry parameters from each visit's deep-dive analysis, listed in Table 1. We fit all observations jointly with priors on the orbital eccentricity ($e\cos\omega$ and $e\sin\omega$) and fixed orbital parameters taken from the fits to all prior transit and RV data done by the RWDDT Scheduling Team with `juliet` (Espinoza et al., 2019). We also tested uninformative priors on the eccentricity parameters. We fit for the eclipse depth, our main parameter of interest, in two ways: 1) Assuming a single eclipse depth shared between each visit and 2) individual, independent depths fit visit-by-visit. Our astrophysical parameter priors are summarized in Table 2.

We define our initial systematics model as $S(t)$:

$$S(t) = P(t)R(t)Y\Big(y(t)\Big)X\Big(x(t)\Big)SY\Big(sy(t)\Big)SX\Big(sx(t)\Big), \quad (1)$$

where

$$P(t) = c_0 + c_1(t - \bar{t})$$

is a linear trend in time where $\bar{t}$ is the mean time,

$$R(t) = 1 + r_0 \exp\Big(-r_1(t - t_{\rm start})\Big)$$

is an exponential ramp where $t_{\rm start}$ is the time of the first integration. Each of Y, X, SY, SX are linear decorrelation functions defined similarly to each other as

$$Y\Big(y(t)\Big) = 1 + c_y\Big(y(t) - \overline{y}\Big)$$

where ($x(t)$, $y(t)$) is the measured centroid position as a function of time, and ($sx(t)$, $sy(t)$) is the measured PSF width along the x- and y-axes as a function of time, and ($\overline{x}$, $\overline{y}$) is the time-averaged centroid position, and ($\overline{sx}$, $\overline{sy}$) is the time-averaged PSF size. We also initially tested the use of a GP. Finally, we also included a multiplicative white noise scalar, $\sigma_{\rm mult}$, to account for any white noise levels beyond the initial Poisson-dominated noise level estimate made by Eureka! (Bell et al., 2022). Priors, fixed parameter values, and free parameter information for the systematics model parameters are listed in Table 3. Because of the range of ramp-effect magnitudes, we also evaluated the trimming of the initial integrations, testing values of 50, 500, 700, and 800 integrations.

Table 1: Aperture photometry parameters used for each visit.

Observation	Aperture Radius (pix)	Sky Inner Annulus (pix)	Sky Outer Annulus (pix)
1	4	14	44
2	8	24	34
3	5	18	46
4 & 5	5	24	54

Table 2: Prior and best-fit astrophysical parameters for the fiducial fit with a minimum systematics model and 700-integration trimming for observations 1-4. Gaussian priors are denoted as $\mathcal{N}(\mu, \sigma)$.

Parameter	Prior	Best Fit Value
$R_{\rm p}/R_*$	Fixed	0.03045
$F_{\rm p}/F_*$ (ppm)	$\mathcal{N}(100, 300)$	$142.5^{+17.9}_{-20.1}$
P (days)	Fixed	2.6162643243
t_0 (BMJD$_{\rm TDB}$)	Fixed	58955.8965273919
b	Fixed	0.5259044225
a/R_*	Fixed	17.2974955329
$e\cos\omega$	$\mathcal{N}(-0.0386, 0.0926)$	$-0.0056^{+0.0007}_{-0.0021}$
$e\sin\omega$	$\mathcal{N}(-0.1443, 0.1542)$	$0.1385^{+0.1009}_{-0.2384}$
$R_*/R_\odot$	Fixed	0.315

Table 3: Prior and best-fit systematic parameters for the fiducial fit with a minimum systematics model and 700-integration trimming for observations 1-4. Gaussian priors are denoted as $\mathcal{N}(\mu, \sigma)$ and Uniform priors as $\mathcal{U}(l, u)$. Systematic parameters are listed for each eclipse observation.

Parameter	Prior	Best Fit Value
c_0 (Visit 1)	$\mathcal{N}(0.999, 0.01)$	$0.99983^{+0.00002}_{-0.00003}$
c_0 (Visit 2)	$\mathcal{N}(0.999, 0.01)$	$0.99986^{+0.00003}_{-0.00012}$
c_0 (Visit 3)	$\mathcal{N}(0.999, 0.01)$	$0.99986^{+0.00002}_{-0.00003}$
c_0 (Visit 4)	$\mathcal{N}(0.999, 0.01)$	$0.99986^{+0.00002}_{-0.00003}$
c_0 (Visit 5)	$\mathcal{N}(0.999, 0.01)$	$0.99986^{+0.00002}_{-0.00002}$
c_1 (Visit 1)	$\mathcal{N}(0.0, 0.1)$	$-0.0131^{+0.0005}_{-0.0005}$
c_1 (Visit 2)	$\mathcal{N}(0.0, 0.1)$	$-0.0017^{+0.0014}_{-0.0004}$
c_1 (Visit 3)	$\mathcal{N}(0.0, 0.1)$	$-0.0019^{+0.0004}_{-0.0003}$
c_1 (Visit 4)	$\mathcal{N}(0.0, 0.1)$	$-0.0023^{+0.0003}_{-0.0004}$
c_1 (Visit 5)	$\mathcal{N}(0.0, 0.1)$	$0.0016^{+0.0008}_{-0.0008}$
r_0 (Visit 1)	$\mathcal{N}(0.0, 0.01)$	$0.00057^{+0.00009}_{-0.00008}$
r_0 (Visit 2)	$\mathcal{N}(0.0, 0.01)$	$0.00008^{+0.00029}_{-0.00016}$
r_0 (Visit 3)	$\mathcal{N}(0.0, 0.01)$	$0.00029^{+0.00009}_{-0.00010}$
r_0 (Visit 4)	$\mathcal{N}(0.0, 0.01)$	$-0.00005^{+0.00011}_{-0.00010}$
r_0 (Visit 5)	$\mathcal{N}(0.0, 0.01)$	$0.00098^{+0.00014}_{-0.00015}$
r_1 (Visit 1)	$\mathcal{U}(3, 300)$	$55.4^{+16.6}_{-13.5}$
r_1 (Visit 2)	$\mathcal{U}(3, 300)$	$59.6^{+152.8}_{-49.7}$
r_1 (Visit 3)	$\mathcal{U}(3, 300)$	$58.9^{+63.5}_{-31.0}$
r_1 (Visit 4)	$\mathcal{U}(3, 300)$	$170.2^{+62.9}_{-72.8}$
r_1 (Visit 5)	$\mathcal{U}(3, 300)$	$204.2^{+43.7}_{-47.3}$
$y_{\rm width}$ (Visit 1)	$\mathcal{N}(0.0, 0.5)$	$0.0158^{+0.0077}_{-0.0083}$
$y_{\rm width}$ (Visit 2)	$\mathcal{N}(0.0, 0.5)$	$0.0175^{+0.0091}_{-0.0081}$
$y_{\rm width}$ (Visit 3)	$\mathcal{N}(0.0, 0.5)$	$0.0309^{+0.0070}_{-0.0065}$
$y_{\rm width}$ (Visit 4)	$\mathcal{N}(0.0, 0.5)$	$0.0170^{+0.0090}_{-0.0084}$
$y_{\rm width}$ (Visit 5)	$\mathcal{N}(0.0, 0.5)$	$0.0299^{+0.0110}_{-0.0110}$
$x_{\rm width}$ (Visit 1)	$\mathcal{N}(0.0, 0.5)$	$-0.0092^{+0.0097}_{-0.0084}$
$x_{\rm width}$ (Visit 2)	$\mathcal{N}(0.0, 0.5)$	$0.0252^{+0.0086}_{-0.0089}$
$x_{\rm width}$ (Visit 3)	$\mathcal{N}(0.0, 0.5)$	$0.0316^{+0.0067}_{-0.0068}$
$x_{\rm width}$ (Visit 4)	$\mathcal{N}(0.0, 0.5)$	$0.0107^{+0.0080}_{-0.0096}$
$x_{\rm width}$ (Visit 5)	$\mathcal{N}(0.0, 0.5)$	$0.0323^{+0.0109}_{-0.0098}$
$\sigma_{\rm mult}$ (Visit 1)	$\mathcal{U}(0.8, 10)$	$1.140^{+0.014}_{-0.012}$ (767^{+9}_{-8} ppm)
$\sigma_{\rm mult}$ (Visit 2)	$\mathcal{U}(0.8, 10)$	$1.195^{+0.013}_{-0.012}$ (804^{+9}_{-8} ppm)
$\sigma_{\rm mult}$ (Visit 3)	$\mathcal{U}(0.8, 10)$	$1.180^{+0.011}_{-0.011}$ (794^{+7}_{-7} ppm)
$\sigma_{\rm mult}$ (Visit 4)	$\mathcal{U}(0.8, 10)$	$1.205^{+0.014}_{-0.015}$ (811^{+9}_{-10} ppm)
$\sigma_{\rm mult}$ (Visit 5)	$\mathcal{U}(0.8, 10)$	$1.166^{+0.015}_{-0.017}$ (784^{+10}_{-11} ppm)

1.3 Results

Table 4 lists the eclipse depths measured with both shared and individual fits, fitted with different systematics models, and with different numbers of integrations trimmed from the beginning of the observations. For the "shared" fits, the orbital parameters and eclipse depths are shared across all observations, while for the "individual" fits we shared the orbital parameters across all observations but allowed for visit-dependent eclipse depths.

Our initial fit to all four eclipses used the full systematics model described in Equation 1 with trimming of the first 50 integrations in each observation (including Observation 5); this resulted in a relatively high shared eclipse depth of 193^{+18}_{-19} ppm. Our fit allowing for visit-dependent eclipse depths and with the same level of trimming showed that the high joint eclipse depth is driven by Observation 1 and Observation 3, with depths of 305^{+32}_{-32} ppm and 186^{+29}_{-30} ppm, respectively. Both of these visits had relatively large ramps at the beginning of the observations and large amounts of red noise indicated by a binning analysis, motivating further time-series trimming. In what follows, we trim different numbers of integrations from Observations 1-4, while only removing the first 50 integrations from Observation 5 which exhibited far weaker settling systematics given that it was immediately preceded by Observation 4.

In early fits to the data with 50-integration trimming, we tested the use of a GP as part of the systematics model. The best-fit value of 105^{+55}_{-39} ppm was about 2σ smaller than the 50-integration trimmed reduction without a GP, described above. Simultaneously the uncertainties were about 2.5 times larger than the non-GP fit, ultimately bringing it within 1σ of our final fiducial reduction with 700-integration trimming, described below, suggesting that the GP was able to mitigate the bias from the ramp effects that necessitated the large number of integrations trimmed, however this came at the expense of precision in the measured eclipse depth.

We next tested whether the full systematics model in Equation 1 was necessary to fit the observations robustly. Both centroid position detrending parameters, $x(t)$ and $y(t)$, had best-fit coefficients that were consistent zero. When we removed these parameters from the fit, we obtained a shared eclipse depth (with 50 integration trimming) of 191^{+18}_{-17} ppm, consistent with the value from the full systematics model of 193^{+18}_{-19} ppm. We continue with this "minimum systematics model" for the rest of the analysis.

At 500 integrations trimmed,[1] the best-fit shared eclipse depth decreases by over 50 ppm compared to the 50-integration trimming to 139^{+19}_{-20}, which is much closer to the zero-albedo, zero-redistribution eclipse depth of the planet of 145 ppm. Again, the individual visit-dependent eclipse depths show higher values for Observations 1 and 3 compared to Observations 2 and 4/5. With increased numbers of integrations trimmed, the red noise is significantly reduced, especially for Observations 1 and 3. Subsequent trimming at 700 and 800 integrations resulted in the shared eclipse depth leveling out to 142^{+18}_{-20} and 146^{+21}_{-21} ppm, respectively, with the individual eclipse depths becoming consistent with one another. We choose a trimming of 700 integrations as our fiducial value as it balances the need to mitigate ramp effects while preserving as many integrations in the fit as feasible — the eclipse depth uncertainty already appears to start increasing for the 800 integration trimming in the minimum systematics model due to so many integrations being thrown away.

[1] We keep Observation 5 trimming at 50 integrations throughout.

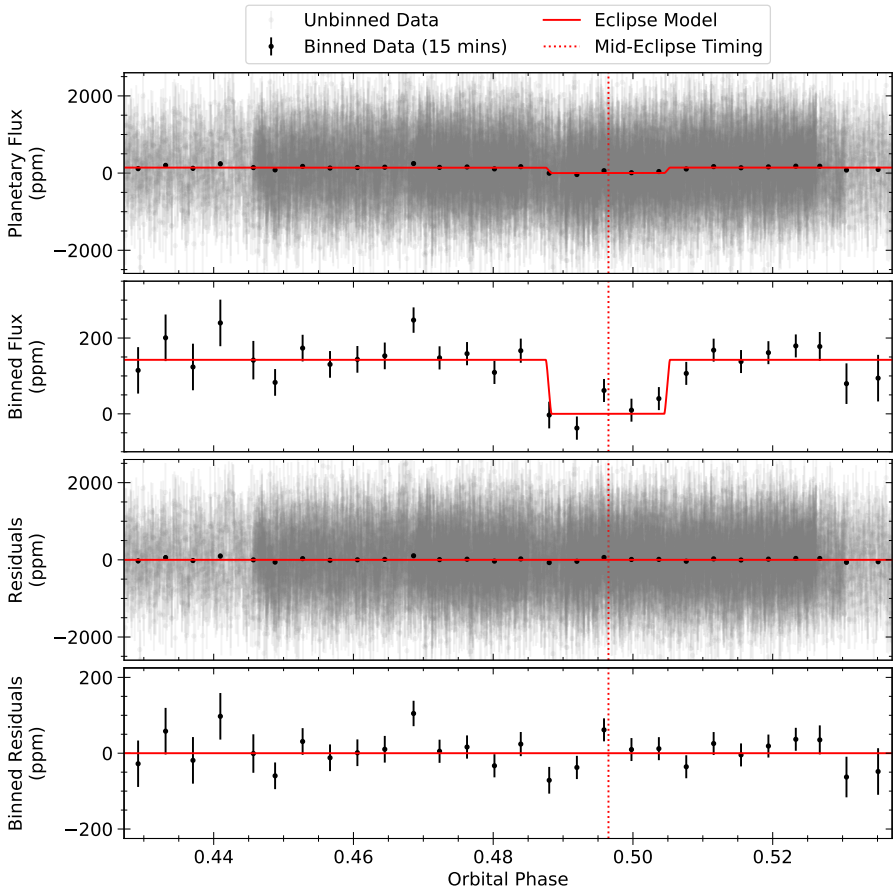

Figure 1: Phase-folded eclipse observations of GJ 3929 b, with integration-level observations in gray and 15-minute temporally-binned data in black, our fiducial 700-integration-trimmed fitted eclipse model in red, and the fitted mid-eclipse orbital phase indicated with a red, dotted vertical line.

Table 4: Combined shared eclipse depths across systematics models and individual visit eclipse depths for different levels of time-series trimming.

Trimming	Shared Eclipse Depth (ppm)			Individual Eclipse Depths (ppm)				
(Integrations)	Full Model	Min. Model	GP Model	Obs 1	Obs 2	Obs 3	Obs 4	Obs 5
50	193^{+18}_{-19}	191^{+18}_{-17}	105^{+55}_{-39}	305^{+32}_{-32}	113^{+30}_{-32}	186^{+29}_{-30}	-1^{+293}_{-334}	98^{+66}_{-69}
500	150^{+17}_{-17}	139^{+19}_{-20}	—	188^{+43}_{-41}	106^{+34}_{-35}	179^{+35}_{-34}	135^{+224}_{-237}	50^{+74}_{-72}
700	142^{+19}_{-19}	142^{+18}_{-20}	—	168^{+39}_{-44}	109^{+32}_{-33}	162^{+33}_{-29}	62^{+204}_{-233}	78^{+67}_{-61}
800	147^{+18}_{-19}	146^{+21}_{-21}	—	160^{+45}_{-50}	97^{+33}_{-34}	159^{+33}_{-31}	-105^{+158}_{-151}	78^{+59}_{-62}

Note: Individual eclipse depths for the 50 and 500 integration trimming rows were done with the full systematics model, while the minimum systematics model was used when trimming 700 and 800 integrations. We also kept Observation 5 trimming at 50 integrations throughout, as Observations 4 & 5 were linked visits targeting the fourth eclipse of GJ 3929 b. Relatedly, Observation 4 appears not to have captured any of the fourth eclipse, and hence its individual eclipse depth constraints are largely prior-dominated, while Observation 5's individual eclipse depth constraint is weakened because it captured only a partial eclipse because the eclipse started during the gap between Observations 4 & 5.

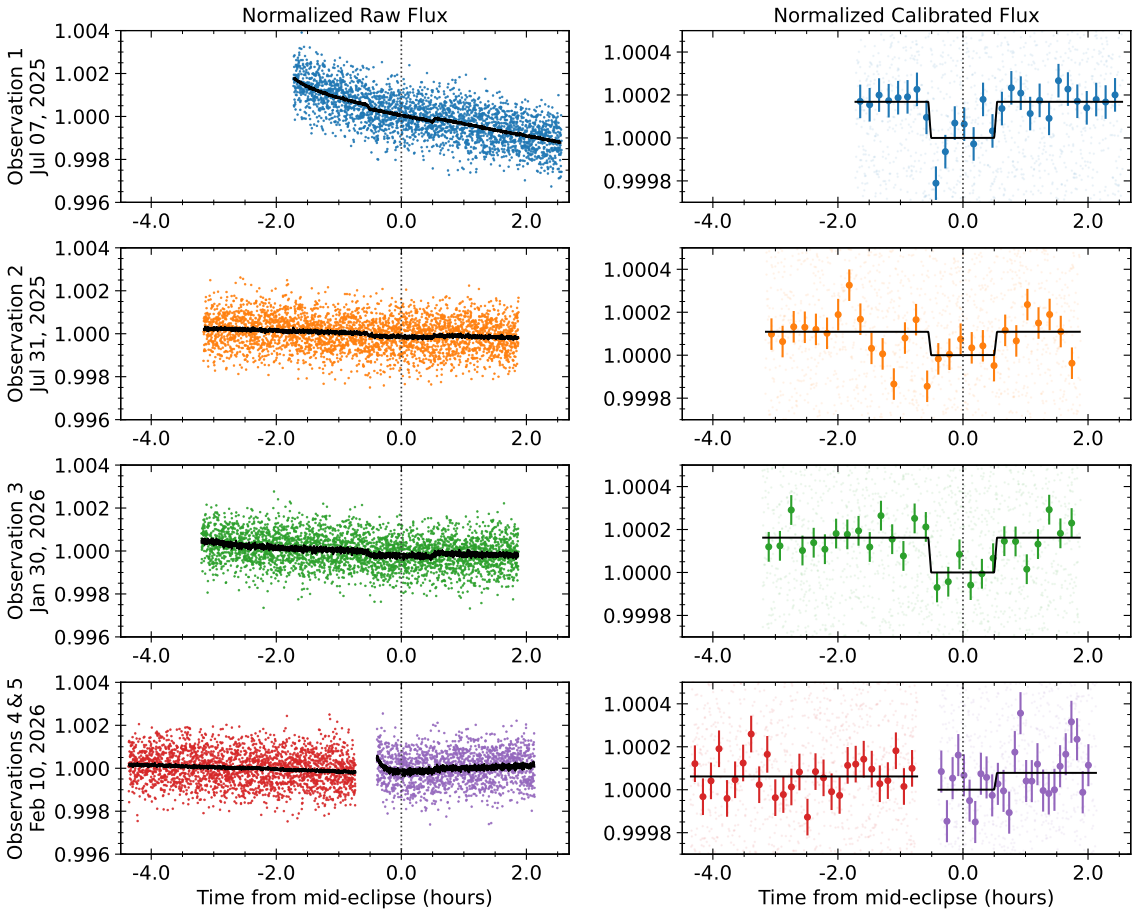

Figure 2: Individual eclipse observations and their corresponding fits, with orbital parameters shared between observations but eclipse depths allowed to vary between observations. *Left:* Normalized, raw flux measurements are shown with colored points, while the fitted astrophysical $\times$ systematics model is shown with black points. *Right:* Normalized, systematics-removed measurements are shown in pale colored dots, 15-minute temporally-binned measurements are shown as large colored circles with error bars, and the fitted eclipse model is shown in black.

Finally, we tested fits using wider eccentricity priors. While the fiducial analysis finds a $e\cos\omega$ value consistent with the Gaussian priors obtained from the RWDDT Scheduling Team via fits to the transit+RV data of the GJ 3929 bsystem, the $e\sin\omega$ values are about 3σ away from the central value of the prior (see Table 2). For eclipse-only observations, the orbit's $e\cos\omega$ can be constrained by the mid-eclipse timing, while the orbit's $e\sin\omega$ is more weakly constrained by our by the eclipse duration through the mapping of impact parameter to the orbital inclination and orbital distance (Winn, 2010). Nonetheless, we conducted a fit with minimally-informative eccentricity priors, where both $e\sin\omega$ and $e\cos\omega$ were allowed to vary uniformly between -1 and 1. In this scenario, we find a shared eclipse depth of 136^{+22}_{-23} ppm and $e\cos\omega$ of $-0.0046^{+0.001}_{-0.003}$, consistent with values found when using the tighter eccentricity priors. The final $e\sin\omega$ posterior is not well-constrained and is mostly a lower-limit, with a median value of 0.41 and a 1σ (2σ) sigma lower-limit of -0.03 (-0.25). We therefore chose to use the solution from the fits with the tighter eccentricity prior as our final answer, as it includes information from the transit and RV fits.

2 Conclusions

Here we present an analysis of the four eclipses of GJ 3929 bfrom the Rocky Worlds Director's Discretionary Time program. Our fiducial analysis (trimming the first 700 integrations from Observations 1–4 and 50 integrations from Observation 5, and using the minimum systematics model) obtains a final eclipse depth of 142^{+18}_{-20} ppm. This is consistent with the zero-albedo, zero-redistribution eclipse depth expected for GJ 3929 b of 145 ppm (Espinoza et al., in prep.). Our fiducial constraints on the planet's eccentricity ($e\cos\omega = -0.0056^{+0.0007}_{-0.0021}$) indicate a non-zero eccentricity at the $> 2\sigma$ level, with the inferred mid-eclipse timing occurring 13.6 ± 3.7 minutes **before** the circular-orbit mid-eclipse time (after accounting for the $\sim$0.4-minute difference in the light travel time between mid-transit and mid-eclipse). We will now cease observations of GJ 3929 b, and observations of the remaining RWDDT sample will proceed.

References

Bell, T., Ahrer, E.-M., Brande, J., et al. 2022, The Journal of Open Source Software, 7, 4503, doi: 10.21105/joss.04503

Espinoza, N., Kossakowski, D., & Brahm, R. 2019, MNRAS, 490, 2262, doi: 10.1093/mnras/stz2688

Winn, J. N. 2010, in Exoplanets, ed. S. Seager (University of Arizona Press), 55–77, doi: 10.48550/arXiv.1001.2010